

Origin of the electrophoretic force on DNA in solid-state nanopores

Stijn van Dorp¹, Ulrich F. Keyser^{2,3}, Nynke H. Dekker¹, Cees Dekker¹ and Serge G. Lemay^{1*}

Despite gel electrophoresis being one of the main workhorses of molecular biology, the physics of polyelectrolyte electrophoresis in a strongly confined environment remains poorly understood. Theory indicates that forces in electrophoresis result from interplay between ionic screening and hydrodynamics^{1,2}, but these ideas could so far be addressed only indirectly by experiments based on macroscopic porous gels. Here, we provide a first direct experimental test by measuring the electrophoretic force on a single DNA molecule threading through a solid-state nanopore³ as a function of pore size. The stall force gradually decreases on increasing the nanopore diameter from 6 to 90 nm, inconsistent with expectations from simple electrostatics and strikingly demonstrating the influence of the hydrodynamic environment. We model this process by applying the coupled Poisson–Boltzmann and Stokes equations in the nanopore geometry^{4,5} and find good agreement with the experimental results.

Voltage-driven transport of macromolecules through biological^{6,7} and artificial^{8–12} nanopores provides an ideal system for studying the physics of the translocation process¹³. Electrophoretic migration is the main driving force for DNA translocation through nanopores and is a consequence of the force exerted by an externally applied electric field on the charges on the polyelectrolyte chain. As DNA in solution is negatively charged, it is screened by a layer of more or less mobile, positively charged counterions that also experience the electric field. It has long been recognized that the force exerted on the counterions induces a hydrodynamic drag force on the DNA that locally balances the electrical force, leading to much slower migration than would be expected from Stokes drag alone (see, for example, ref. 1). The electrophoretic translocation of a polymer through a small pore obeys similar principles, but here the geometry of the pore (or the local structure of the gel) is expected to profoundly influence the hydrodynamic flow profile around the DNA and thereby the drag force opposing movement^{1,5,14}. Despite increasingly sophisticated experiments^{3,12,15,16}, an unambiguous manifestation of hydrodynamic interactions in DNA translocation has not yet been reported. Here, we address this issue using our recently developed apparatus combining solid-state nanopores with optical tweezers³ to arrest DNA translocation, and subsequently measure the stalling force on a single DNA strand (see the Methods section). A schematic diagram of the measurement apparatus is shown in Fig. 1a.

In contrast with a gel electrophoresis experiment, the electric field in a nanopore experiment is confined to the immediate vicinity of the pore and electrical forces act locally on a short segment of the DNA. The electric field strength in the pore typically reaches $\sim 10^6$ V m⁻¹ owing to the very thin (~ 60 nm) free-standing membranes. The large persistence length of λ -DNA,

about 50 nm, ensures that the DNA segment inside the pore is practically fully extended. The situation is depicted schematically in Fig. 1b, where L and R represent the length and radius of the pore and ΔV is the applied potential. DNA has a bare line charge density $\lambda_{\text{bare}} = -0.96$ nC m⁻¹ (2 electrons per base pair) and is modelled here as a uniformly charged cylinder with radius $a = 1.1$ nm. The bare electrostatic force on the DNA backbone is represented by $F_{\text{bare}} = \lambda_{\text{bare}} \Delta V$ (ref. 3). It is opposed by a drag force F_{drag} caused by the electrophoretic motion of its counterions in the opposite direction: F_{drag} is thus an intrinsic component of the translocation process that is also ultimately traceable to electrical forces⁵. The resulting net force is the electrophoretic force driving the translocation, given by $F_{\text{elec}} = F_{\text{bare}} - F_{\text{drag}}$. In our case, F_{elec} is balanced by an opposing mechanical force $F_{\text{mech}} = -F_{\text{elec}}$ from the optical tweezers that arrests the DNA inside the pore.

The origin of F_{drag} lies in the spatial distribution of the ions and the corresponding fluid flow profile. A mean-field description of the ion distributions is given by the Poisson–Boltzmann formalism, in which the electrostatic potential is given by $\nabla^2 \bar{\Phi}(r) = \lambda_{\text{D}}^{-2} \sinh \bar{\Phi}(r)$ and the corresponding ion distributions as $n_{\pm}(r) = n_0 e^{\pm \bar{\Phi}(r)}$. Here, λ_{D} is the Debye length, $\bar{\Phi} = -e\Phi/k_{\text{B}}T$ is the reduced electrostatic potential, e is the elementary charge, Φ is the potential, k_{B} is the Boltzmann constant, T is the temperature, n is the number density of ions and z is the valency of the ionic species. Figure 2a shows calculated potentials $\bar{\Phi}$ for two pore sizes obtained by numerical evaluation of the Poisson–Boltzmann equation in a cylindrical geometry (see the Methods section). The corresponding ion distributions are shown in Fig. 2b. The Debye layer of the DNA is characterized by a depletion of coions, whereas counterions pile up to very high densities owing to the high DNA charge. As these distributions are solutions to the full (nonlinearized) Poisson–Boltzmann equation, the effect of Manning condensation¹⁷ is included.

In our DNA stalling experiment, the distribution of the counterions largely determines the velocity profile of the induced electro-osmotic flow. The flow velocity profile can be calculated by solving the Stokes equation $\eta \nabla_r^2 v_z = E_z \rho(r)$, where η is the dynamic viscosity of the fluid, v_z is the fluid velocity, E_z is the applied electric field and $\rho(r)$ is the ionic charge distribution. Calculated fluid flow profiles are shown in Fig. 2c. Subsequently, to relate the flow profile to viscous drag, the shear stress in the fluid is calculated as $\tau(r) = -\eta(dv_z/dr)$. Figure 2d shows $\bar{\tau} = 2\pi r \tau / \lambda_{\text{bare}}$, which is equal to the ratio $F_{\text{drag}}/F_{\text{bare}}$ when evaluated at the DNA surface ($r = a$). It shows that F_{drag} is of the same order of magnitude as the bare electrostatic force acting on the DNA that it opposes. F_{drag} is larger for the larger pore, corresponding to a smaller stalling force.

For comparison with our experiments, it is convenient to express the above model in a form that directly relates the

¹Kavli Institute of Nanoscience, Delft University of Technology, 2628 CJ Delft, The Netherlands, ²Institut für Experimentalphysik I, Universität Leipzig, 04103 Leipzig, Germany, ³Cavendish Laboratory, University of Cambridge, Cambridge CB3 0HE, UK. *e-mail: s.g.lemay@tudelft.nl.

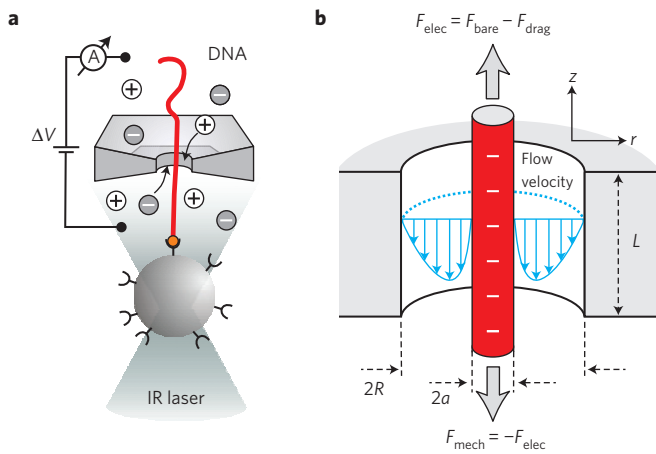


Figure 1 | Experimental configuration. **a**, Schematic diagram of the measurement apparatus. Using optical tweezers, DNA translocation is stalled and the force on the DNA is measured. The nanopore ionic conductance is also measured simultaneously. **b**, Cylindrical model of DNA in a nanopore. The blue arrows on either side of the DNA schematically depict the velocity of the moving fluid due to electro-osmosis.

electrophoretic force to the properties of the nanopore. As was shown previously⁵, the Poisson–Boltzmann and Stokes equations can be combined to yield an expression for the electrophoretic force on a stationary molecule,

$$F_{\text{elec}} = -F_{\text{mech}} = \frac{2\pi\epsilon [\Phi(a) - \Phi(R)]}{\ln(R/a)} \Delta V \quad (1)$$

$\Phi(a)$ and $\Phi(R)$ are the surface potentials of the DNA and the nanopore, respectively, and ϵ is the dielectric constant of water. $\bar{\Phi}(a)$ and $\bar{\Phi}(R)$ deduced from the Poisson–Boltzmann equation are plotted in Fig. 2e as a function of R . In large pores, the surface potentials are independent of R . Equation (1) then predicts that the measured force F_{mech} has a simple $\ln^{-1}(R/a)$ dependence on the size of the pore. In smaller pores, on the other hand, the Debye layer is compressed by the pore wall (Fig. 2). This results in a dependence of the surface potentials on the pore size and a correspondingly more complicated dependence of F_{mech} on R .

A way to directly test the above model is to measure the DNA stalling force F_{mech} as a function of the pore radius R . As previous work has focused on smaller pores, however, we first demonstrate that it is possible to detect the presence of a single DNA molecule in very large ($R \gg a$) nanopores. The detection of DNA in the pore is based on measuring the step in ionic conductance ΔG when DNA enters the pore. ΔG was previously shown to be caused by competition between two contributions: volume exclusion, lowering the number of ions available for conductance, and an excess of DNA counterions, effectively increasing the number of ions available for conductance¹². Which of these two effects dominates depends on the bulk concentration of electrolyte, causing ΔG to be positive (conductance increase) in the present experiments with 20–50 mM salt. Under these optimized salt conditions, the signal-to-noise ratio of DNA capture is predicted to be high even in very large pores¹⁸. A typical step in the current together with the corresponding change in position Z of the bead is shown in Fig. 3a. We observe a clear step in the current even though the DNA changes the conductance of the nanopore by less than 1%. A typical histogram of capture events is shown in Fig. 3b. These data show that we are able to controllably insert and detect single molecules even in nanopores with $R = 45$ nm, where the DNA covers only 1/2000th of the nanopore cross-sectional area.

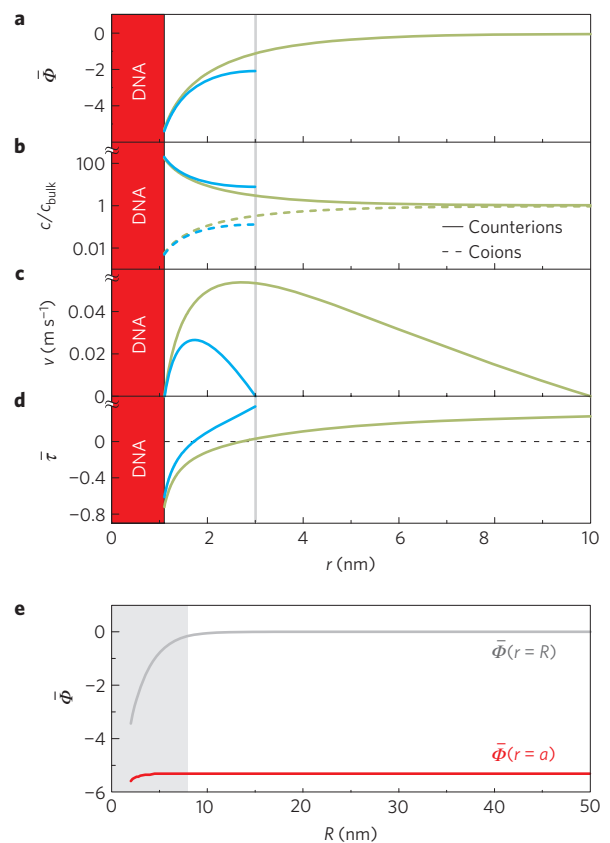


Figure 2 | Mean-field calculations. **a**, Reduced electrostatic potential for a ‘large’ pore (green, $R = 10$ nm) and a ‘small’ pore (blue, $R = 3$ nm). The grey line indicates the location of the pore wall for the small pore. The salt concentration is $c_{\text{bulk}} = 20$ mM ($\lambda_D = 2.2$ nm) and the pore walls are taken as uncharged in this particular calculation for simplicity. **b**, Corresponding ion distributions. In ‘large’ pores ($R \gg \lambda_D$), the distribution of ions around the DNA is not significantly affected by the pore wall, as indicated by the observation that the green curves reach the bulk value. However, in ‘small’ pores ($R \lesssim \lambda_D$), the counterion cloud (solid curves) is compressed by the pore wall and the pore can be depleted of coions (dashed curves), leaving mainly positive counterions to balance the negative charges on the DNA. This situation is exemplified by the blue curves. **c**, Fluid velocity profiles calculated by combining results from **a** and **b** with the Stokes equation. **d**, Normalized surface integral of the shear stress at each position r , calculated as $\bar{\tau} = -2\pi r \tau / \lambda_{\text{bare}}$, with τ being the shear stress in the fluid. At the DNA surface, $\bar{\tau} = F_{\text{drag}} / F_{\text{bare}}$. **e**, Calculated reduced surface potentials for DNA (red) and nanopore wall (grey) as a function of the pore radius. The grey area qualitatively depicts the ‘small pore’ region, in which the ion distributions are influenced by the confinement of the nanopore.

Experimentally determined ΔG values as a function of nanopore radius are shown in Fig. 3c for 10 nanopores with radii ranging from $R = 3$ to 45 nm. The grey area indicates the ‘small pore’ region in which, according to the calculations in Fig. 2b, the ion distributions near the DNA are influenced by the presence of the nanopore wall. In apparent concurrence with the simulations, ΔG is approximately constant in large nanopores. The larger ΔG in small nanopores is consistent with the compression of the diffuse screening layer, ensuring charge neutrality in the pore. A more quantitative comparison of the measured ΔG with theory is difficult, however: the access resistance R_{acc} becomes an increasingly important contribution to the total resistance of the system in large pores¹⁹, and it is currently unknown how the presence of DNA threading through the pore affects R_{acc} .

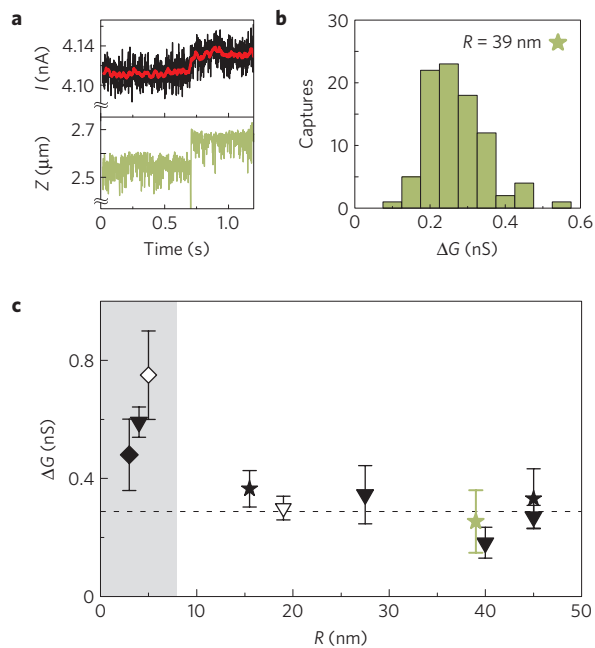


Figure 3 | Conductance change due to DNA capture. **a**, Typical example of pore current I (upper panel, red averaged) and bead position Z (lower panel) during DNA capture in an $R = 39$ nm pore in 33 mM KCl at 80 mV. Current measurements were low-pass filtered at 1 kHz. **b**, Histogram of ΔG of 88 DNA captures in the nanopore under the same conditions as in **a**. **c**, ΔG in pores of different radii. Capture events typically occurred at voltages of 60–100 mV. The horizontal dashed line is a guide to the eye. Triangles: 20 mM KCl, stars: 33 mM KCl, diamonds: 50 mM KCl, green star: data from **b**, error bars: standard deviation evaluated from ΔG histograms. The open symbols represent data from free translocation experiments without optical tweezers.

Having established the feasibility of arresting and detecting DNA molecules in large as well as small pores, we now turn to the main result of this letter, namely, the experimentally determined magnitude of the stalling force F_{mech} as function of the nanopore radius R . Figure 4a shows F_{mech} as a function of applied voltage ΔV in nanopores with $R = 4$ nm (left panel) and $R = 39$ nm (right panel). This relationship is approximately linear in both cases. However, $F_{\text{mech}}/\Delta V$ in the small pore is a factor of two larger than in the large pore. Figure 4b shows the ratio $F_{\text{mech}}/\Delta V$ as a function of pore size: $F_{\text{mech}}/\Delta V$ decreases gradually with increasing size, as expected on the basis of equation (1). The dashed curve results from combining the surface potentials for the full DNA charge (Fig. 2e) with equation (1), without any extra adjustments. In spite of the inherent simplifications of a one-dimensional model, the theoretical result captures the trend in the data quite well, although it quantitatively overestimates the stalling force by $\sim 50\%$. This difference can be attributed to (a combination of) several factors, including a reduction of counterion mobility at the DNA surface^{12,20}, or an extra opposing electro-osmotic fluid flow resulting from fixed charges on the nanopore surface⁵. In terms of equation (1), both effects can be represented by lowering the magnitude of the surface potential difference $\Delta\Phi = \Phi(a) - \Phi(R)$, thereby reducing the magnitude of F_{mech} . Empirically reducing $\Delta\Phi$ by 33% results in the solid curve in Fig. 4b, an excellent fit to the experimental data. This reduction of $\Delta\Phi$ is equivalent to approximately 50% of the DNA's bare charge being screened by ions that are effectively immobilized on its surface (as shown in Supplementary Fig. S1) or to the presence of a 15 mC m^{-2} surface charge on the pore wall (Supplementary Fig. S2). Although our experiment

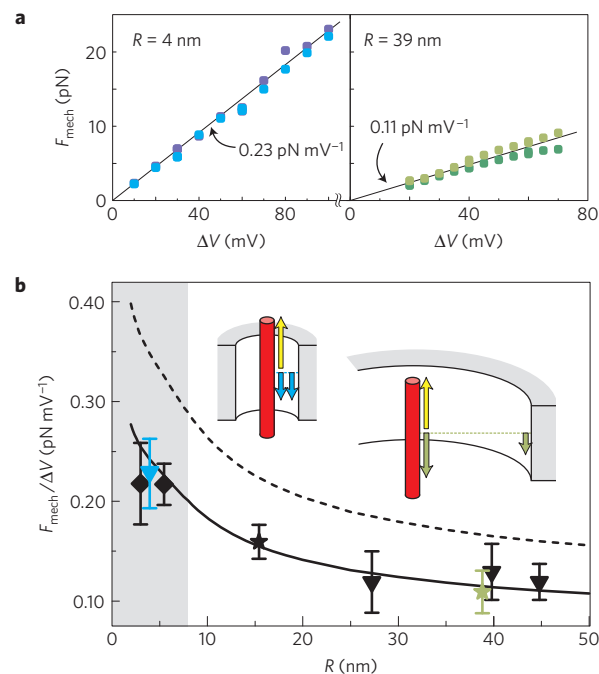


Figure 4 | Pore-size dependence of the DNA stalling force.

a, Measurements of the stalling force as a function of the applied potential in a small (left panel) and a large nanopore (right panel). In each case, two measurements obtained at different distances between the bead and the nanopore are shown. **b**, Measured force versus pore radius. The blue and green symbols correspond to data in **a**. The data in the small-pore area were taken from ref. 3. The curves represent the theoretical result for the bare DNA charge (dashed curve) and for a reduced $\Delta\Phi$ (solid line, see text). The inset shows schematically how the force on the DNA counterions is divided between the DNA and the pore walls through viscous drag in a small and a large pore; the yellow arrow represents the bare electrostatic force acting on the DNA. Triangles: 20 mM KCl, stars: 33 mM KCl, diamonds: 50 mM KCl. Error bars stem from the uncertainties in the calibration of the optical trap, which are estimated at 10–30% of the calibrated trap stiffness.

cannot directly distinguish between these two mechanisms, the inferred surface charge density is typical for SiO_2 surfaces²¹. This suggests that the surface charge density in our nanopores is not strongly influenced by the fabrication process and that the pore charge is responsible for a substantial part of the observed correction.

External factors not taken into account in our simple model might affect the absolute value of the stalling force as well. For example, it might be biased by electrostatic and/or hydrodynamic forces on the bead or on the portion of the DNA residing in the electric field just outside the nanopore. However, our experiments show no evidence for such effects, as we detected no change in the stalling force when the bead was positioned at increasing distances from the nanopore³. In addition, experimental force–voltage curves are linear in our voltage range (Fig. 4a), indicating that entropic forces are small compared with the electrostatic forces, consistent with independent measurements of the entropic forces in DNA stretching²².

The dependence of the measured force on pore radius in Fig. 4b directly demonstrates that the electrophoretic force in DNA translocation is in part determined by hydrodynamic coupling between the DNA's counterions and the nanopore wall. The nanopore geometry determines the magnitude of the drag force exerted on the DNA by these counterions. This coupling has important consequences for the interpretation of experimentally determined

forces because these forces are manifestly not determined by the intrinsic properties of the DNA alone^{1,23}.

Variations of the force can also be expected with increasing salt concentration because this changes the Debye length and thereby both the DNA surface potential and presumably the stalling force F_{mech} . This expectation is however complicated by the facts that the pore surface charge density also changes considerably with salt concentration¹² and that the mean-field theory used here becomes unreliable at high ionic strength. In previous experiments, F_{mech} was in fact found to be independent of salt concentration up to 1 M (ref. 3), and an interpretation of those data based on a model in which $\Phi(R)$ depends on salt concentration was suggested by Ghosal⁵.

In free DNA translocation, the restoring force F_{mech} is absent and effectively replaced by an extra Stokes drag F_{Stokes} proportional to the velocity of the molecule. The molecule translocates at constant velocity, the electrophoretic force being balanced by F_{Stokes} . The relation between the stalling force F_{mech} , as measured with the optical tweezers, and the translocation velocity v_{trans} , as determined from free DNA translocation experiments, is given by^{4,5,14}

$$F_{\text{mech}} = \eta \frac{2\pi L}{\ln(R/a)} v_{\text{trans}} \quad (2)$$

This result is equivalent to the Stokes drag that would be experienced by an uncharged cylinder translocating through a cylindrical pore at constant velocity v_{trans} . Thus, F_{mech} and v_{trans} are proportional quantities, related by a geometry-dependent factor. This expectation is qualitatively confirmed by experimental data^{3,12}, which show that F_{mech} and v_{trans} are indeed roughly proportional. Calculating v_{trans} as the λ -DNA contour length divided by the experimentally determined translocation time gives $v_{\text{trans}} = (16 \mu\text{m}/1.1 \text{ ms}) \approx 15 \text{ mm s}^{-1}$, resulting in $F_{\text{mech}}/v_{\text{trans}} = 1,750 \text{ pN s m}^{-1}$ (data for 5-nm-radius pores). Equation (2) however gives a value of 249 pN s m^{-1} for this factor, using $\eta = 1 \times 10^{-3} \text{ N s m}^{-2}$, $L = 60 \text{ nm}$, $R = 5 \text{ nm}$ and $a = 1.1 \text{ nm}$. This is seven times lower than the experimentally obtained value. Translocation of DNA through these pores therefore occurs at a much lower velocity than expected from the electrophoretic forces measured with the optical tweezers and the mean-field description. As similar nanopores were used in all of these experiments, this conclusion points to a more fundamental difference between the static situation of a stalled molecule and the dynamic situation of a translocating molecule. In free DNA translocation, the conformation of the DNA outside the pore results in extra drag on the moving molecule²⁴, which may account for the discrepancy.

In conclusion, we have shown that the electrophoretic force on a DNA molecule in a nanopore depends on the geometry of the pore. This is not expected from simple electrostatics but can be understood straightforwardly by considering the hydrodynamic drag induced by the counterions screening the DNA in solution. Numerical calculations based on mean-field equations yield a good description of the pore-size dependence of the measured forces.

Methods

Experimental procedures. The nanopores are fabricated by drilling and subsequently expanding holes with $\sim 1 \text{ nm}$ accuracy in a 60-nm-thick $\text{SiO}_2/\text{SiN}/\text{SiO}_2$ membrane using a transmission electron microscope²⁵. The experimental apparatus has been described elsewhere²⁶ and is shown schematically in Fig. 1a. In brief, a microfluidic sample cell containing the nanopore is mounted on an inverted microscope. A standard current amplifier (Axon 200b, Molecular Devices) is used to detect the presence of single DNA molecules in the nanopore. An optical trap required for the force measurements is created by coupling an infrared laser (wavelength 1,064 nm) into the microscope objective. In the trap, micrometre-sized beads coated with DNA molecules (λ -DNA, length = 48.6 kb) are held in close proximity to the nanopore until a single DNA molecule is captured electrophoretically by the nanopore^{3,27}. The translocation is subsequently stalled

by the restoring force of the optical trap. The force measurements are carried out with a typical distance of 5 μm between the bead and the nanopore. The optical trap is aligned above the centre of the nanopore with accuracy of a few tens of nanometres²⁸. In all experiments, the solution has pH = 8.0 set by adding 1 mM of TrisHCl-EDTA.

Modelling. Converging numerical solutions to the nonlinear Poisson–Boltzmann equation in one-dimensional geometries were obtained using the COMSOL Multiphysics package (COMSOL, Inc.) and a custom MATLAB script (The Mathworks, Inc.). One boundary condition was determined by the charge density on the DNA, where $d\Phi/dr = -\lambda_{\text{bare}}/2\pi a\epsilon$. A second boundary condition depended on the properties of the nanopore surface. Nanopores composed of SiO_2 are typically negatively charged, leading to an extra liquid flow opposite to the direction of motion of the DNA. To simplify the discussion, the nanopore walls were assumed uncharged in the calculations of Fig. 2. The situation including charged walls is however described in Supplementary Fig. S2. The boundary condition on the insulating pore wall was thus taken as $d\Phi/dr = 0$. All of the calculations were carried out for monovalent symmetric electrolyte with bulk concentration $c_{\text{bulk}} = 20 \text{ mM}$.

Received 14 October 2008; accepted 18 February 2009; published online 29 March 2009

References

- Long, D., Viovy, J. L. & Ajdari, A. Stretching DNA with electric fields revisited. *Biopolymers* **39**, 755–759 (1996).
- Viovy, J. L. Electrophoresis of DNA and other polyelectrolytes: Physical mechanisms. *Rev. Mod. Phys.* **72**, 813–822 (2000).
- Keyser, U. *et al.* Direct force measurements on DNA in a solid-state nanopore. *Nature Phys.* **2**, 473–477 (2006).
- Ghosal, S. The effect of salt concentration on the electrophoretic speed of a polyelectrolyte through a nanopore. *Phys. Rev. Lett.* **98**, 238104 (2007).
- Ghosal, S. Electro-kinetic-flow-induced viscous drag on a tethered DNA inside a nanopore. *Phys. Rev. E* **76**, 061916 (2007).
- Kasianowicz, J., Brandin, E., Branton, D. & Deamer, D. Characterization of individual polynucleotide molecules using a membrane channel. *Proc. Natl Acad. Sci. USA* **93**, 13770–13773 (1996).
- Meller, A., Nivon, L. & Branton, D. Voltage-driven DNA translocations through a nanopore. *Phys. Rev. Lett.* **86**, 3435–3438 (2001).
- Li, J. *et al.* Ion-beam sculpting at nanometre length scales. *Nature* **412**, 166–169 (2001).
- Li, J., Gershow, M., Stein, D., Brandin, E. & Golovchenko, J. DNA molecules and configurations in a solid-state nanopore. *Nature Mater.* **2**, 1611–1615 (2003).
- Chang, H. *et al.* DNA-mediated fluctuations in ionic current through silicon oxide nanopore channels. *Nano Lett.* **4**, 1551–1556 (2004).
- Storm, A., Chen, J., Zandbergen, H. & Dekker, C. Translocation of double-strand DNA through a silicon oxide nanopore. *Phys. Rev. E* **71**, 051903 (2005).
- Smeets, R. *et al.* Salt dependence of ion transport and DNA translocation through solid-state nanopores. *Nano Lett.* **6**, 89–95 (2006).
- Dekker, C. Solid-state nanopores. *Nature Nanotech.* **2**, 209–215 (2007).
- Ghosal, S. Electrophoresis of a polyelectrolyte through a nanopore. *Phys. Rev. E* **74**, 041901 (2006).
- Wanunu, M., Sutin, J., McNally, B., Chow, A. & Meller, A. DNA translocation governed by interactions with solid state nanopores. *Biophys. J.* **95**, 4716–4725 (2008).
- Levy, S., Mannion, J., Cheng, J., Reccius, C. & Craighead, H. Entropic unfolding of DNA molecules in nanofluidic channels. *Nano Lett.* **8**, 3839–3844 (2008).
- Manning, G. The molecular theory of polyelectrolyte solutions with applications to the electrostatic properties of polynucleotides. *Q. Rev. Biophys.* **11**, 179–246 (1978).
- Smeets, R., Keyser, U., Dekker, N. & Dekker, C. Noise in solid-state nanopores. *Proc. Natl Acad. Sci. USA* **105**, 417–421 (2008).
- Hall, J. Access resistance of a small circular pore. *J. Gen. Physiol.* **66**, 531–532 (1975).
- Netz, R. Polyelectrolytes in electric fields. *J. Phys. Chem.* **107**, 8208–8217 (2003).
- Behrens, S. & Grier, D. The charge of glass and silica surfaces. *J. Chem. Phys.* **115**, 6716–6721 (2001).
- Wang, M., Yin, H., Landick, R., Gelles, J. & Block, S. Stretching DNA with optical tweezers. *Biophys. J.* **72**, 1335–1346 (1997).
- Luan, B. & Aksimentiev, A. Effective screening of the DNA charge in a nanopore. *Phys. Rev. E* **78**, 021912 (2008).
- Storm, A. *et al.* Fast DNA translocation through a solid-state nanopore. *Nano Lett.* **4**, 1193–1197 (2005).
- Storm, A., Chen, J., Ling, X., Zandbergen, H. & Dekker, C. Fabrication of solid-state nanopores with single-nanometre precision. *Nature Mater.* **2**, 537–540 (2003).

26. Keyser, U., van der Does, J., Dekker, C. & Dekker, N. Optical tweezers for force measurements on DNA in nanopores. *Rev. Sci. Instrum.* **77**, 105105 (2006).
27. Trepagnier, E., Radenovic, A., Sivak, D., Geissler, P. & Liphardt, J. Controlling DNA capture and propagation through artificial nanopores. *Nano Lett.* **7**, 2824–2830 (2007).
28. Keyser, U. *et al.* Nanopore tomography of a laser focus. *Nano Lett.* **5**, 2253–2256 (2005).

Acknowledgements

We are grateful to M.-Y. Wu and R. Smeets for the fabrication of the nanopores and to Y.-H. Chien and S. Hage for the preparation of the DNA constructs. We acknowledge

J. van der Does for assistance with construction of the experimental set-up. This work was supported by NWO, FOM and the Emmy Noether Program of the DFG.

Author contributions

Conceived experiments: S.v.D., U.F.K., N.H.D., C.D. and S.G.L. Carried out experiments and analysed data: S.v.D. and U.F.K. Wrote paper: S.v.D., U.F.K., N.H.D., C.D. and S.G.L.

Additional information

Supplementary information accompanies this paper on www.nature.com/naturephysics. Reprints and permissions information is available online at <http://npg.nature.com/reprintsandpermissions>. Correspondence and requests for materials should be addressed to S.G.L.